High-Temperature Phase Transformations in Al-Li-Cu-Mg-Zr-Sc Alloy Studied by In-Situ Electron Microscopy

Rostislav Králík , Lucia Bajtošová , Barbora Kihoulou , Dalibor Preisler , Miroslav Cieslar *

Posted Date: 16 January 2024

doi: 10.20944/preprints202401.1153.v1

Keywords: Al-Cu-Li-Mg-Sc-Zr alloy; in-situ TEM; homogenization; primary phase particles; twin-roll casting; mold-casting

Article

High-Temperature Phase Transformations in Al-Li-Cu-Mg-Zr-Sc Alloy Studied by In-Situ Electron Microscopy

Rostislav Králík, Lucia Bajtošová, Barbora Kihoulou, Dalibor Preisler and Miroslav Cieslar *

Faculty of Mathematics and Physics, Charles University, Ke Karlovu 5, 12116, Prague 2, Czechia; rostislav.kralik@matfyz.cuni.cz (R.K.); lucibajtos@gmail.cz (L.B.); barbora.krivska@matfyz.cuni.cz (B.K.); dalibor.preisler@mff.cuni.cz (D.P.); miroslav.cieslar@mff.cuni.cz (M.C.)

* Correspondence: miroslav.cieslar@mff.cuni.cz (M.C.)

Abstract: A homogenization of billets from Al-Cu-Li-Mg-Sc-Zr alloys should be accomplished at high annealing temperatures exceeding 500 °C. This type of aluminum alloy is susceptible to the depletion of surface layers from Li. Therefore, choosing a suitable homogenization temperature and duration is a crucial step in assuring a homogeneous distribution of alloying elements and optimal exploitation of the potential of the alloy. In-situ heating in an electron microscope was performed on a twin-roll cast Al-Cu-Li-Mg-Sc-Zr alloy to understand the peculiarities of the homogenization process. Four types of primary phase particles rich in Cu, Li, Mg, and Fe were identified in the as-cast material. They appear as coarse particles at the boundaries of eutectic cells. Their partial dissolution occurs at temperatures above 450 °C. They are almost fully dissolved at 550 °C, except for complex phases containing Fe and Cu. Small dimensions of eutectic cells in the range of 10 μm assure a homogeneous distribution of main alloying elements within the matrix after 20 min of annealing. Direct comparison with the same material prepared by mold-casting indicates that such short annealing times result in the dissolution of main primary phase particles but do not assure a homogeneous distribution of alloying elements in the whole volume of the specimen.

Keywords: Al-Cu-Li-Mg-Sc-Zr alloy; in-situ TEM; homogenization; primary phase particles; twin-roll casting; mold-casting

1. Introduction

Al-Cu-Li-Mg-based alloys are promising materials widely used in aerospace components thanks to their superior mechanical properties and good corrosion resistance. The Li addition secures the low density and the high elastic modulus of the materials [1,2]. In the case of the newest generation of Al-Li-based alloys, only a reduced concentration of Li (0.75 to 1.8 wt. %) is kept [3]. This composition suppresses the formation of metastable δ′ Al_3Li precipitates [4], which is responsible for anisotropic material properties and poor fatigue performance [5], and instead favors the formation of other strengthening phases. In Al-Li-Cu alloys, they are primarily Cu-based phases - binary θ' (Al_2Cu) and ternary T_1 (Al_2CuLi) as well as T_2 (Al_6CuLi_3) [6,7]. The precipitation of T_1 could be further stimulated by adding alloying elements such as Ag or Mg, which reduce stacking fault energy, retard recovery, and thus promote precipitation of the T_1 phase on extended dislocations [8]. A further advantage of Mg addition is a decrease in the total density and precipitation of a rod-like strengthening S' (Al_2CuMg) phase [9].

Recrystallization, texture control, and fatigue improvement are achieved by adding Zr, or Zr and Sc, which form fine Al_3Zr or Al_3(Zr, Sc) dispersoids [10]. On the other hand, the presence of Fe impurities generally leads to the formation of an insoluble constituent Al_7Cu_2Fe phase [11].

Conventional methods of sheet production from the Al-Cu-Li-Mg-based alloys start with the employment of ingot casting methods such as direct-chill (DC) casting, vacuum induction casting (VIC), or mold casting (MC) under a protective atmosphere. Ingot-cast materials exhibit inhomogeneous solute distribution on a macroscopic level and contain coarse constituent particles.

 doi:10.20944/preprints202401.1153.v1

Dissolving the coarse particles and homogeneous distribution of the constituent elements is necessary to achieve peak hardening from the precipitating phases. For this reason, homogenization annealing is first performed after the casting of the material before forming, solution treatment, and age hardening [12–14].

For homogenization and primary phase dissolution, long-term homogenization (16 -24 hours) at high annealing temperatures (above 500 °C) is required [15–18]. However, in the case of Al-Li-based alloys, such long-term high-temperature annealing induces the evaporation of Li from the surface [19] and the formation of Li-depleted layers. Scalping of Li-depleted surface layers is then necessary and generates a considerable amount of waste. Moreover, fine Sc-containing dispersoids, which generally form between 300-480 °C, are prone to coarsening at homogenization temperatures [20] and lose their advantageous effects once they coarsen beyond the coherency limit. This coarsening could be significantly suppressed in alloys micro-alloyed with Zr [13]. However, some Al_3(Zr, Sc) dispersoid growth was consistently observed, even at relatively low annealing temperatures (<500 °C) [21,22].

Alternative methods of thin strips or thick sheets of the Al-Cu-Li-Mg-Zr-based material preparation can be employed to reduce the duration of homogenization at high temperatures. Continuous casting methods, including twin roll casting (TRC), are promising [23,24]. Due to high solidification rates related to this method, much finer primary constituent particles are formed, and the segregation scales are much lower. Consequently, solute homogenization and primary phase dissolution are possible at significantly shorter annealing times, diminishing the undesirable effects of homogenization annealing of ingot-cast materials, namely the coarsening of Al_3(Sc, Zr) dispersoids and Li surface evaporation.

In this work, specimens of TRC Al-Cu-Li-Mg-Zr-Sc alloy were annealed in-situ in a scanning transmission electron microscope (STEM), and the transformation and dissolution of primary phase particles were monitored. Comparison with mold-cast material was carried out. In-situ experiments, including the possibility of phase analysis directly at selected annealing temperature using ACOM-TEM, are a powerful tool enabling direct visualization of the transformation of the as-cast structure.

2. Materials and Methods

Alloy with the composition given in Table 1 was used as input material for preparing TRC and MC materials. Concentrations of respective elements represent average values received from three measurements in both TRC and MC billets. Details of the preparation of TRC materials can be found in [25]. MC was performed under an argon protective atmosphere to an air-cooled graphite mold of 110 × 56 × 26 mm^3. Irregularities and surface impurities of ingots were scalped to obtain a final block 85 × 50 × 22 mm^3, which was used for further processing and study. The chemical composition of both alloys was received from optical emission spectrometry (Q4 TASMAN).

Table 1. Average composition of TRC and MC materials in wt. %.

Element	Cu	Li	Mg	Zr	Sc	Ag	Ti	V	Fe	Al
Concentration	2.6	0.7	0.27	0.1	0.2	0.3	0.01	0.01	0.1	bal.

Discs with 3 mm diameter were mechanically ground on SiC papers and electrolytically polished in a twin-jet TENUPOL V at -16 °C with a 33 % solution of HNO3 in methanol. Transmission electron microscopy and scanning transmission electron microscopy (TEM/STEM) observations were done in JEOL JEM 2200 FS electron microscope in TEM and STEM modes using bright field (BF) and high-angle annular dark field (HAADF). The Gatan heating stage for TEM was used for step-by-step in-situ heating with the step 50 °C/20 min. EDX characterizations of initial and annealed TRC specimens were performed at room temperature (annealed specimens were cooled to room temperature in the TEM heating stage with a cooling rate of 200 °C / min). The TEM is equipped with "Spinning Star" electron precession from NanoMEGAS with an ASTAR software package for the automated orientation phase mapping (ACOM-TEM) and the acquisition of orientation maps.

 doi:10.20944/preprints202401.1153.v1

Due to the size of eutectic cells in the MC material, the microscope was operated in low magnification mode in STEM during the in-situ experiment. Initial and post-mortem observations of MC material, EDX mapping, and BSE observations were done in the FEI Quanta scanning electron microscope (SEM).

3. Results

3.1. As-cast structures

Because the high-temperature behavior of ingot-cast Al-Li alloys is well described in the literature [12–14], only brief characterizations were performed in the present study. The microstructure of the MC material consists of polyhedral eutectic cells with particles of primary phases at their boundaries. Figure 1 shows typical SEM images and EDX maps of the main alloying elements in the material. Coarse Cu-rich primary phase particles are located along the boundaries of eutectic cells. The detected chemical composition indicates the presence of θ-Al_2Cu or T_1-Al_2CuLi phases. The presence of Mg could not be reliably excluded because the local concentrations in particles are very similar to the ones in the bulk of the material. Most probably, the S-Al_2CuMg phase is also present in boundary phases. An increased concentration of Cu is apparent in an approximately 1ten micrometers broad area around the primary phases (Figure 1c – white arrows). This concentration gradient between the grain boundary and its interior is a direct effect of the eutectic solidification of the alloy [26]. Additionally, smaller (below 5 μm) Fe-rich particles, most probably of the Al_7Cu_2Fe phase [27], appear in several parts of the boundary of the eutectic cell (Figure 1d).

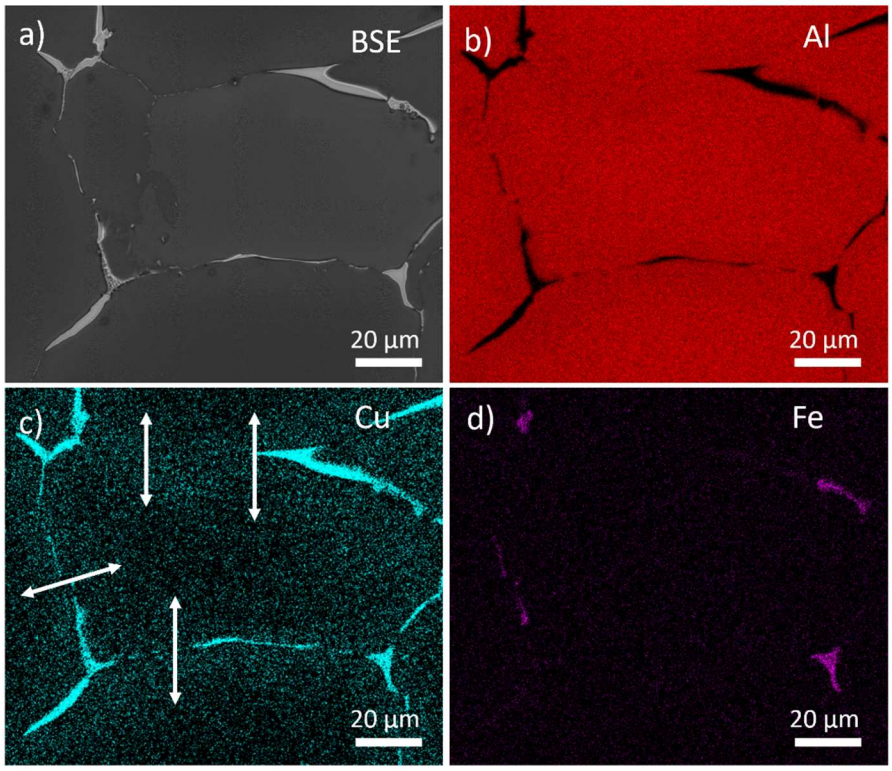

Figure 1. Distribution of elements in as-cast MC alloy. SEM BSE image of the primary phases a). Corresponding EDS maps b-d).

Generally, as-cast TRC materials exhibit finer cell size, finer dispersion of primary particles, and higher solid solution supersaturation [28]. Figure 2 shows two examples of boundary particles in a thicker part of the TEM specimen (~500 nm). A noticeable gradient in Cu concentration observed in MC material (Figure 1c) is not evident (Figure 2 c,h). The brighter part (higher intensity of inelastically scattered electrons) near particles in the HAADF contrast (Figure 2 a,f) represents only parasitic thickness modifications due to the inhomogeneous distribution of potentials during the

Preprints (www.preprints.org) | NOT PEER-REVIEWED | Posted: 16 January 2024 doi:10.20944/preprints202401.1153.v1

electropolishing of the specimen. Nevertheless, an elevated concentration of Mg in several rod-like particles suggests the presence of the S-Al_2CuMg phase.

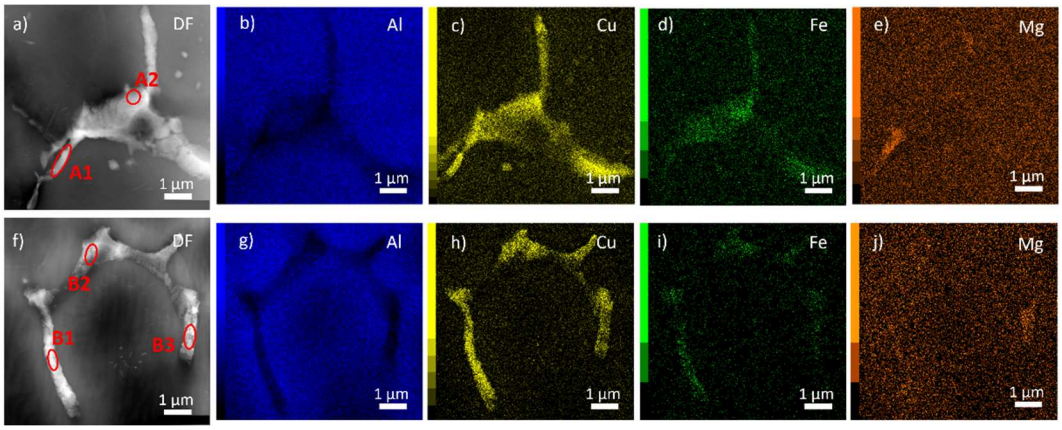

Figure 2. Distribution of main alloying elements in the as-cast TRC alloy. HAADF STEM images a,e). Corresponding EDS maps b)-e), g)-j).

Quantification of the composition was performed in several parts of primary phase particles. Examples are listed in Table 2. Because there is always an overlap of several particles containing Al, Cu, Mg, and Fe, Li cannot be detected by EDX, and particles are embedded in the Al matrix, a direct interpretation of measured concentration is impossible. However, higher concentrations of Cu, Fe, and Mg suggest the existence of large equilibrium θ-Al_2Cu, T_1-Al_2CuLi, or S-Al_2CuMg phases overlapped with smaller particles of Al_7Cu_2Fe phase (concentrations of other elements fell below 0.1 at. %). Statistical diffraction analysis of particles in thinner parts of the specimen using ACOM-TEM proves the presence of θ, S, and T_1 particles (examples in Figures 3, 4, and 5) in the as-cast state. More details about this type of analysis can be found in the work of Bajtošová et al. [29].

Table 2. Concentrations of elements in selected spots of the as-cast TRC material (at. %).

Area	Al	Cu	Fe	Mg
A1	75.4	23.4	0.1	1.2
A2	74.6	23.9	1.0	0.6
B1	47.2	51.1	1.3	0.4
B2	63.6	35.5	0.6	0.3
B3	56.9	35.9	1.4	5.8

Preprints (www.preprints.org) | NOT PEER-REVIEWED | Posted: 16 January 2024 doi:10.20944/preprints202401.1153.v1

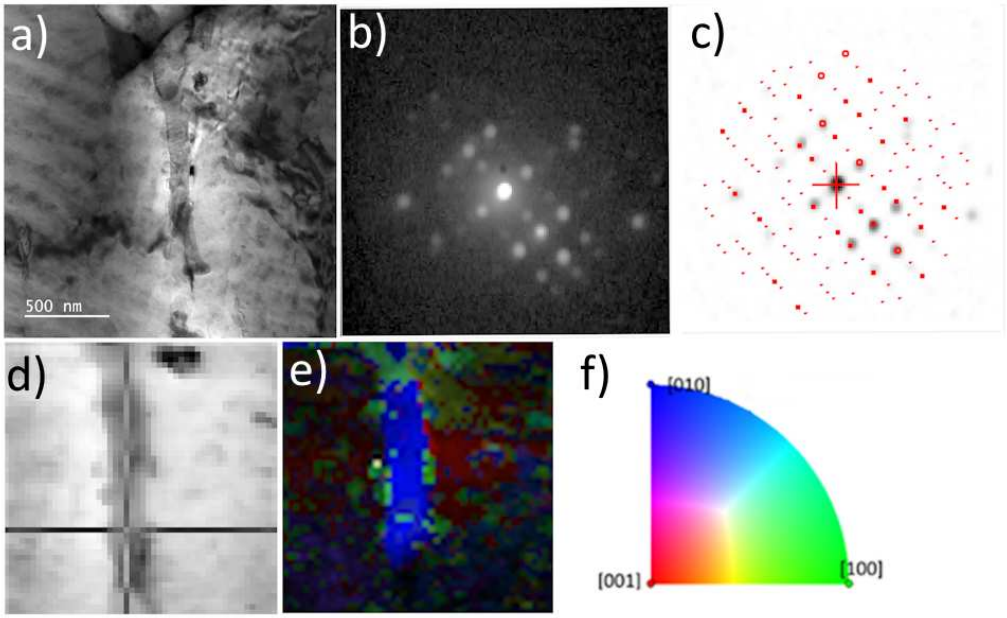

Figure 3. ACOM-TEM analysis of primary centered orthorhombic S-Al_2CuMg phase in as-cast TRC alloy. TEM BF image a), experimental diffraction pattern b) and matching with simulations c), virtual BF d) indicating the acquisition position of the diffraction pattern in c), orientation map e), orientation triangle f).

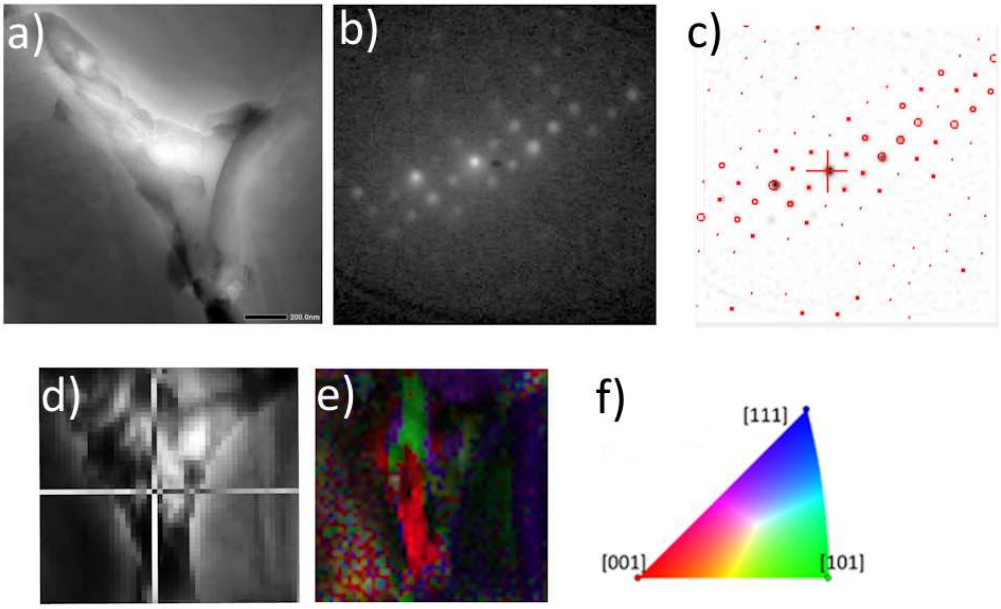

Figure 4. ACOM-TEM analysis of primary body-centered tetragonal θ-Al_2Cu phase in as-cast TRC alloy. TEM BF image a), experimental diffraction pattern b) and matching with simulations c), virtual BF d) indicating the acquisition position of the diffraction pattern in c), orientation map e), orientation triangle f).

Preprints (www.preprints.org) | NOT PEER-REVIEWED | Posted: 16 January 2024 doi:10.20944/preprints202401.1153.v1

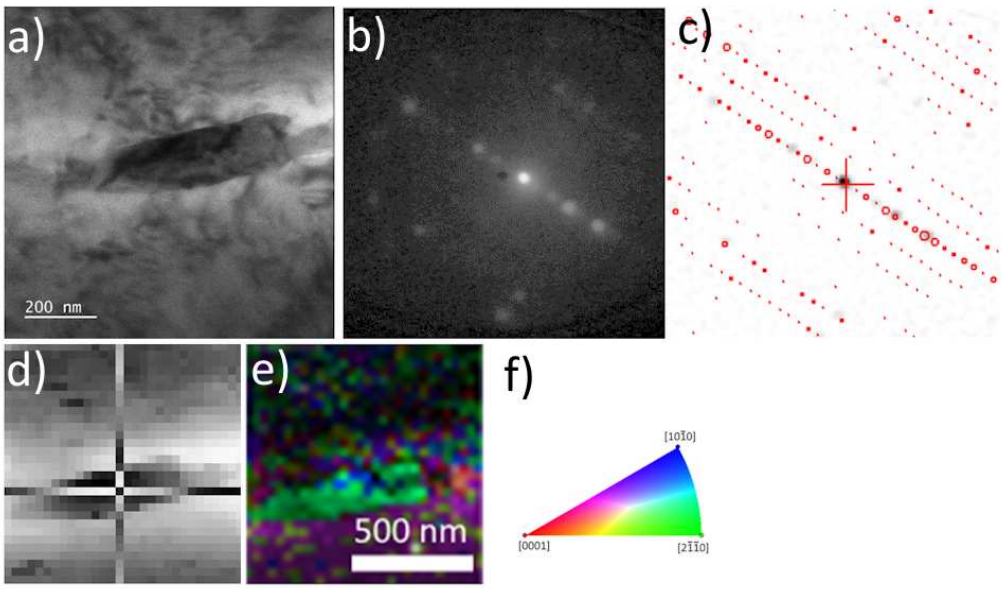

Figure 5. ACOM-TEM analysis of primary hexagonal T_1-Al_2CuLi phase in as-cast TRC alloy. TEM BF image a), experimental diffraction pattern b) and matching with simulations c), virtual BF d) indicating the acquisition position of the diffraction pattern in c), orientation map e), orientation triangle f).

3.2. In-situ annealing

Specimens for this type of measurement were fixed first in the heating stage of the TEM and then step-by-step annealed to final high temperatures. The TEM/STEM microscope was operated in the low magnification SEM mode in MC alloy, using a back-scattered electron detector. The processes in Figure 6 are similar to those observed generally in ingot-cast materials [12]. Primary phase particles remain almost uninfluenced by the annealing up to 500 °C. However, the majority of them dissolve at 560 °C.

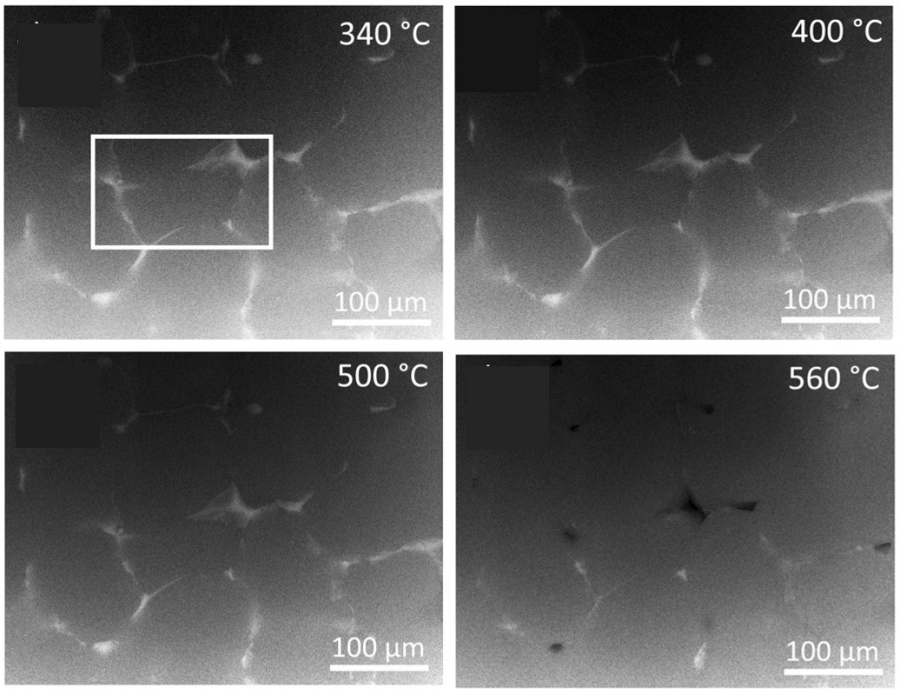

Figure 6. In-situ STEM annealing of MC specimen, BSE detector signal. The white rectangle indicates the area analyzed in the as-cast state (Figure 1).

Preprints (www.preprints.org) | NOT PEER-REVIEWED | Posted: 16 January 2024 doi:10.20944/preprints202401.1153.v1

Closer EDX and SEM analyses (Figure 7) were performed on the same specimen zone as in Figure 1. The specimen was cooled to room temperature first. A relatively low cooling rate (200 K/min) does not preserve the structure formed at high temperatures, and the material exhibits another feature typical for ingot-cast Al-Li-Cu-Mg alloys exposed to elevated temperatures for relatively short times (~ 20 min at 560 °C). While only insoluble Cu and Fe-rich particles (most probably Al_7Cu_2Fe) persist, A part of Cu atoms near the original boundaries of eutectic cells reprecipitate in coarse Cu-rich particles (marked by arrows in Figure 7a). By the literature [27], this limited zone confirms that a homogeneous distribution of Cu could not be reached during such a short annealing period in ingot-cast materials containing relatively large eutectic cells in the as-cast state.

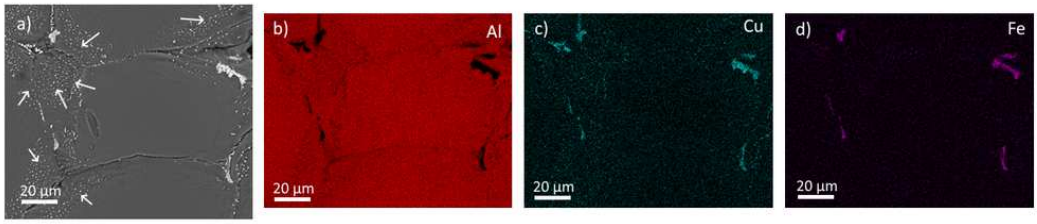

Figure 7. a) SEM BSE image of the highlighted MC specimen area after annealing, b-d) EDS maps.

Primary phase particles in the TRC material are significantly finer than in the MC alloy. Their distribution in smaller eutectic cells strongly impacts the redistribution of main alloying elements during annealing. The evolution of two particles from Figure 2 during this process is demonstrated in Figures 8 and 9. Only precipitation and coarsening of matrix particles known for this system [30,31] occur at temperatures up to 300 °C. The first signs of the segmentation of original particles occur at 400 °C already. It is accompanied by a coarsening of matrix precipitates near the boundaries of eutectic cells, most probably due to the elevated concentration of solute atoms released from boundary particles. A substantial dissolution of matrix particles begins above 450 °C, similar to the dissolution of primary phase particles. However, due to the size of the primary phase particles, their decomposition is finalized at 500 °C. Above this temperature, most boundary phases are dissolved, and the remaining ones go through visible morphological modifications connected with their coalescence and ripening.

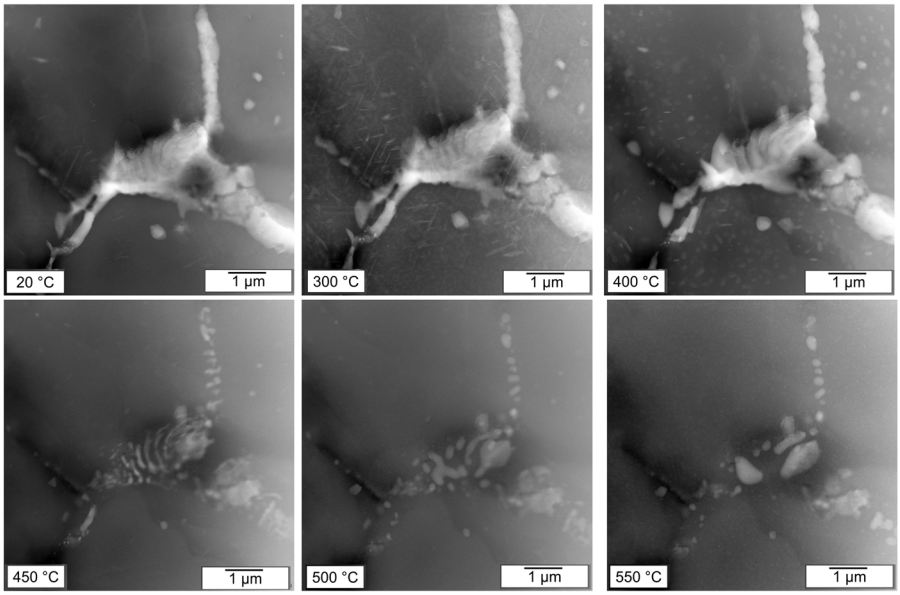

Figure 8. Evolution of primary phase particles in TRC material during in-situ heating. STEM HAADF images.

Preprints (www.preprints.org) | NOT PEER-REVIEWED | Posted: 16 January 2024 doi:10.20944/preprints202401.1153.v1

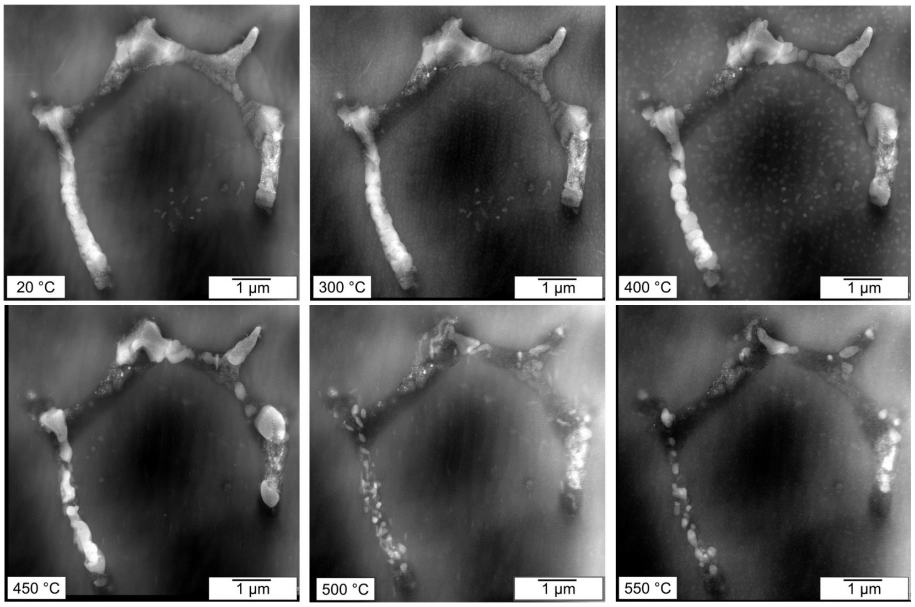

Figure 9. HAADF images of the in-situ annealing experiment of the TRC material.

Figure 10. illustrates the detailed dissolution of one Al_2CuLi primary phase particle in a thinner part of the specimen and the formation of smaller matrix particles at temperatures close to 400 °C and 450 °C. In contrast to EDX characterization, ACOM-TEM analysis is not limited by the elevated temperature. The only limitation is the quality of the diffraction pattern, which might considerably depend on the thickness of the TEM foil and the overlap of several phases. The original Al_2CuLi particle, stable at 400 °C, dissolves at 450 °C and is substituted by stable matrix precipitates even after cooling to room temperature (Figures 10 c,g,k,d,h,l).

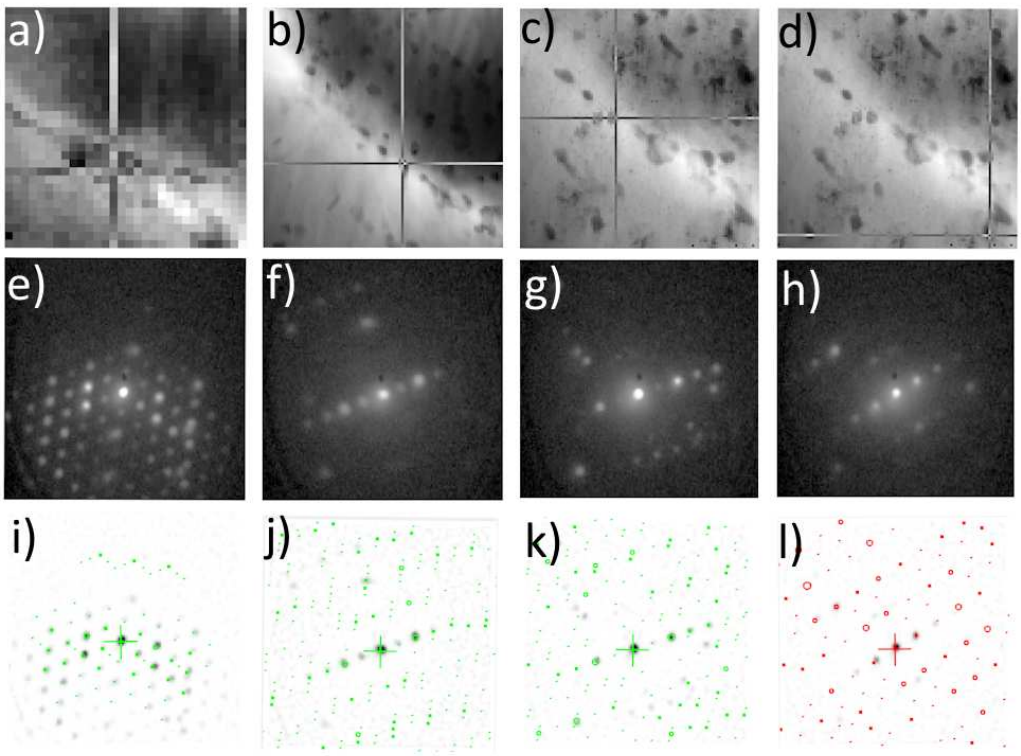

Figure 10. ACOM-TEM analysis of dissolution of primary Al_2CuLi particle. Virtual bright field a,b,c,d), corresponding diffractograms e,f,g,h), and automated phase matching i,j,k,l). Al_2CuLi

Preprints (www.preprints.org) | NOT PEER-REVIEWED | Posted: 16 January 2024 doi:10.20944/preprints202401.1153.v1

primary phase particle a,e,i), Al_2CuLi precipitates b,c,f,g,j,k), and Al_2Cu precipitate d,h,l). 400 °C a,e,i), 450 °C b,f,j), and room temperature c,d,g,h,kl).

Figure 11 and Table 3 show that only complex phases containing Cu and Fe (Al_7Cu_2Fe) remain after annealing at 550 °C and cooling to room temperature. Coarse particles enriched in Cu (D1) or Mg (D3) in Figure 11f appear as an artifact of a limited cooling rate because they do not exist at high temperatures (Figures 8,9).

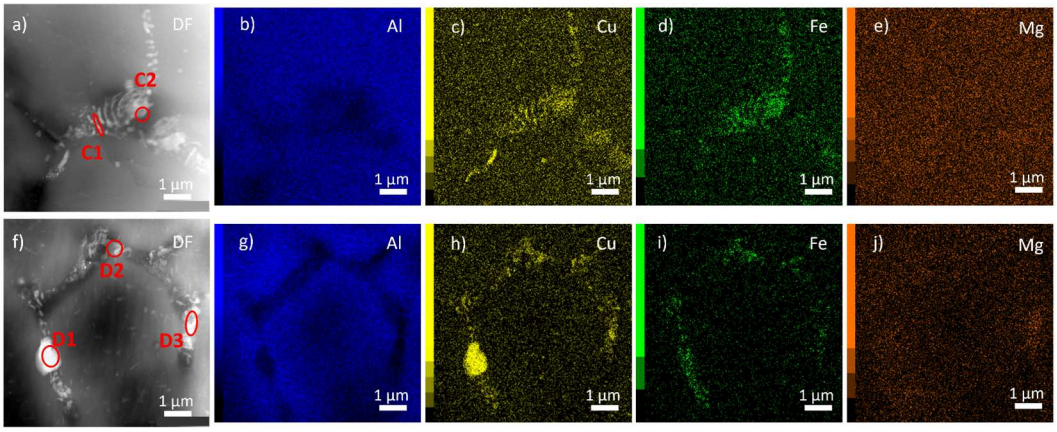

Figure 11. TRC material after annealing up to 550 °C and cooling to room temperature. HAADF STEM images a,f) and corresponding corresponding EDX maps of main alloying elements b-e, g-j).

Table 3. The concentration of elements in selected spots of the in-situ annealed TRC material cooled to room temperature (at. %).

Area	Al	Cu	Fe	Mg
C1	88.8	9.7	1.1	0.5
C2	90.4	6.8	1.8	1.0
D1	46.9	51.2	0.9	1.0
D2	75.8	19.7	2.8	1.8
D3	72.4	20.4	1.0	6.2

4. Discussion

The twin-roll casting of Al-Li-based strips could provide properties not achievable by conventional ingot-casting and downstream processing methods due to significantly higher solidification rates reaching 10^2 - 10^3 K/s [32] compared to units of K/s typical for DC-cast Al alloys [33]. Although the cooling rate in TRC materials is relatively high, eutectic cells with coarse primary phase particles always form, and homogenizing the material at high temperatures is unavoidable. The critical parameter controlling the temperature and duration of this homogenization treatment is the size of eutectic cells or dendrite secondary arm spacing L [24,34]. Generally, they are related to the cooling rate v_c or a local solidification time t_s by a power function [35,36]:

$$L = A.v_c^{-n} \quad (1)$$

$$L = B.t_s^n \quad (2)$$

where n is an empirical factor ranging from 1/3 to 1/2, A and B are material dependent constants. Rough estimations yield the ratio between the cell sizes of the TRC alloy and MC alloy ranging between 5 and 20, which is in good agreement with the structures of our materials (compare Figure 1 and Figure 2).

The in-situ TEM experiment shows, that for a full dissolution of equilibrium θ-(Al_2Cu), T_1-(Al_2CuLi), and S-(Al_2CuMg) phases the homogenization temperature should approach 550 - 560 °C in agreement with the literature data, while the Fe-bearing phase Al_7Cu_2Fe still persists [12,13,24,33].

 doi:10.20944/preprints202401.1153.v1

This temperature transfers the majority of main solute atoms from the cell boundary into the matrix. However, short annealing times in the range of tens of minutes do not guarantee their homogeneous distribution in the original eutectic cell. The diffusion length w defined from the diffusion coefficient D as

$$w = (Dt)^{\frac{1}{2}} \quad (3)$$

where t is the annealing time, and

$$D = D_0 \exp(-\frac{Q}{RT}) \quad (4)$$

is for the slowest element (Cu), about 5 μm at 550 °C and 20 min (D_0= 4.8×10^{-5} m^2/s, $Q = 133.6 \times 10^3 J/mol$, $R= 8.314$ $J/(mol \cdot K)$, and T is the thermodynamic temperature) [12]. This distance well corresponds with the width of the precipitation zone in the MC specimen cooled from the homogenization temperature to room temperature (Figure 7a). The TRC material does not exhibit such well-delimited precipitation zones. The characteristic dimension of the eutectic cell is of the same range as the diffusion length. Therefore, precipitates formed in the cooled specimen (Figure 11f) are homogeneously spread in the whole volume of the original eutectic cell. Longer homogenization duration is necessary for a homogeneous distribution of solutes in the MC material. Estimations based on Equation 3 yield a duration time close to 10 h to guarantee the diffusion length above 25 μm. This value is close to one-half of the eutectic cell size in the MC alloy.

5. Conclusions

The Al-Cu-Li-Mg-Sc-Zr-based alloy prepared by two methods with vastly different solidification rates was investigated during a model in-situ homogenization experiment in TEM. The following conclusions can be deduced from the present study:

- A high solidification rate during twin-roll casting impacts the size of eutectic cells. Their average diameter is in the range of several micrometers. The mold-cast material exhibits a larger cell size by one order of magnitude.
- The primary phase particles situated at cell boundaries were identified by ACOM-TEM and EDX analyses as θ-(Al_2Cu), T_1-(Al_2CuLi), S-(Al_2CuMg), and Al_7Cu_2Fe.
- The Al_7Cu_2Fe phase cannot be dissolved during the homogenization annealing. Only indistinctive morphological changes and ripening occur at temperatures above 500 °C.
- The remaining primary phase particles dissolve in both materials after 20 min holding time at temperatures close to 550 °C. The duration of this annealing is sufficient to distribute the main alloying elements homogeneously in the original eutectic cells in the TRC material. Homogenization times in the range of 10 h would be necessary to receive the same homogeneous distribution in the MC material.
- The observed processes are in good agreement with recent diffusion models.

Author Contributions: Conceptualization: M.C.; Investigation: L.B., R. K., B. K., D.P.; Supervision: M. C.; Visualization: L. B., R. K.; Writing – original draft: R.K., L. B.; Writing – review and editing: R. K., M. C.

Funding: This research was funded by Czech Science Foundation project number 20-19170S and the Charles University Grant Agency project number 938120.

Acknowledgments: The authors would like to acknowledge the assistance of Dr. Olexandr Grydin, Prof. Mirko Schaper, and Dr. Mykhailo Stolbchenko in manufacturing and providing the twin-roll cast materials.

Institutional Review Board Statement: Not applicable.

Data Availability Statement: The original contributions presented in the study are included in the article, further inquiries can be directed to the corresponding author.

Conflicts of Interest: The authors declare no conflicts of interest.

References

1. Prasad, N; Gokhale, A.; Rao, P. Mechanical behavior of aluminium-lithium alloys. *Mat Sci Eng* **2003**, *28*, 209–246. DOI: https://doi.org/10.1007/BF02717134

2. Starke, E. A.; Staley, J. T. Application of modern aluminum alloys to aircraft. *Prog Aerosp Sci* **1996**, *32*, 131-172. DOI: https://doi.org/10.1016/0376-0421(95)00004-6
3. Rioja, R. J.; Liu, J. The Evolution of Al-Li Base Products for Aerospace and Space Applications. *Metall Mater Trans A* **2012**, *43*, 3325-3337. DOI: https://doi.org/10.1007/s11661-012-1155-z
4. Flower, H.; Gregson, P. Solid state phase transformations in aluminium alloys containing lithium. *Mater Sci Technol* **1987**, *3*, 81–90. DOI: https://doi.org/10.1179/mst.1987.3.2.81
5. Venkateswara Rao, K. T.; Ritchie, R. O. Fatigue of Aluminum-Lithium Alloys. *Int Mater Rev* **1992**, *37*, 153-185. DOI: https://doi.org/10.1179/imr.1992.37.1.153
6. Meetsma, A.; Deboer, J. L.; VanSmaalen, S. REFINEMENT OF THE CRYSTAL-STRUCTURE OF TETRAGONAL AL2CU. *J Solid State Chem* **1989**, *83*, 370-372. DOI: https://doi.org/10.1016/0022-4596(89)90188-6
7. Noble, B.; Thompson, G. E. T1 (Al2CuLi) Precipitation in Aluminium–Copper–Lithium Alloys. *Met Sci J* **1972**, *6*, 167-174. DOI: https://doi.org/10.1179/030634572790445975
8. Wang, S. C.; Starink, M. J. Precipitates and intermetallic phases in precipitation hardening Al–Cu–Mg–(Li) based alloys. *Int Mater Rev* **2005**, *50*, 193-215. DOI: https://doi.org/10.1179/174328005X14357
9. Heying, B.; Hoffmann, R-D.; Pottgen, R. Structure Refinement of the S-Phase Precipitate MgCuAl2. *Z Naturschoft* **2005**, *60*, 491-494. DOI: https://doi.org/10.1515/znb-2005-0502
10. Tolley, A.; Radmilovic, V.; Dahmen, U. Segregation in Al3(Sc,Zr) precipitates in Al–Sc–Zr alloys. *Scripta Mater* **2005**, *52*, 621-625. DOI: https://doi.org/10.1016/j.scriptamat.2004.11.021
11. Yu, Ch.; Yin, D.; Zheng, F.; Yu, X. Effects of solution treatment on mechanical properties and microstructures of Al-Li-Cu-Mg-Ag alloy. *J Cent South Univ* **2013**, *20*, 2083-2089. DOI: https://doi.org/10.1007/s11771-013-1710-9
12. Huang, H.; Xiong, W.; Jiang, Z.; Zhang, J. A Quasi In-Situ Study on the Microstructural Evolution of 2195 Al-Cu-Li Alloy during Homogenization. *Materials* **2022**, *15*, 6573. DOI: https://doi.org/10.3390/ma15196573
13. Tang, Y.; Xiao, D.; Huang, L.; You, R.; Zhao, X.; Lin, N.; Ma, Y.; Liu, W. Effect of Minor Sc Addition on the Microstructure Evolution of Al–Cu–Li–Mg Alloy During Homogenization with Different Cooling Modes. *Met Mater Int* **2022**, *28*, 2422-2433. DOI: https://doi.org/10.1007/s12540-021-01146-9
14. Yang, S.; Jian, S.; Xiaodong, Y.; Xiwu, L.; Fei, Z.; Baoging, S. Homogenization Treatment Parameter Optimization and Microstructural Evolution of Al-Cu-Li Alloy. *Rare Metal Mat Eng* **2017**, *46*, 28-34. DOI: https://doi.org/10.1016/S1875-5372(17)30072-3
15. Suresh, M.; Sharma, A.; More, A. M.; Nayan, N.; Suwas, S. Effect of Scandium addition on evolution of microstructure, texture and mechanical properties of thermo-mechanically processed Al-Li alloy AA2195. *J Alloy Compd* **2018**, *740*, 364-374. DOI: https://doi.org/10.1016/j.jallcom.2017.12.045
16. Li, H. Z.; Ou, Y. J.; Liao, H. J.; Liang, X. P.; Jiang, J. Microstructural Evolution of High Purity Al-Cu-Mg Alloy during Homogenization. *Mater Sci Forum* **2014**, *788*, 208-214. DOI: https://doi.org/10.4028/www.scientific.net/MSF.788.208
17. Gazizov, M.; Teleshov, V.; Zakharov, V.; Kaibyshev, R. Solidification behaviour and the effects of homogenisation on the structure of an Al–Cu–Mg–Ag–Sc alloy. *J Alloy Compd* **2011**, *509*, 9497-9507. DOI: https://doi.org/10.1016/j.jallcom.2011.07.050
18. Nayan, N.; Narayana Murty, S. V. S.; Jha, A. K.; Pant, B.; Sharma, S. C.; George, K. M.; Sastry, G. V. S. Processing and characterization of Al–Cu–Li alloy AA2195 undergoing scale up production through the vacuum induction melting technique. *Mat Sci Eng: A* **2013**, *576*, 21-28. DOI: https://doi.org/10.1016/j.msea.2013.03.054
19. Fink, D.; Hnatowicz, V.; Kvitek, J.; Havranek, V.; Zhou, J. T. External oxidation of aluminium-lithium alloys. *Surf Coat Tech* **1992**, *51*, 57-64. DOI: https://doi.org/10.1016/0257-8972(92)90215-V
20. Xu, P.; Jiang, F.; Tang, Z.; Yan, N.; Jiang, J.; Xu, X.; Peng, Y. Coarsening of Al3Sc precipitates in Al-Mg-Sc alloys. *J Alloy Compd* **2019**, *781*, 209-215. DOI: https://doi.org/10.1016/j.jallcom.2018.12.133
21. Wang, Y.; Xiong, B.; Li, Z.; Zhang, Y.; Teng, H. Precipitation Behavior of Al3(Sc,Zr) Particles in High-Alloyed Al–Zn–Mg–Cu–Zr–Sc Alloy During Homogenization. *Arab J Sci Eng* **2021**, *46*, 6027-6037. DOI: https://doi.org/10.1007/s13369-020-05268-x
22. Fuller, C. B.; Murray, J. L.; Seidman, D. N. Temporal evolution of the nanostructure of Al(Sc,Zr) alloys: Part I – Chemical compositions of Al3(Sc1−xZrx) precipitates. *Acta Mater* **2005**, *53*, 5401-5413. DOI: https://doi.org/10.1016/j.actamat.2005.08.016
23. Li. S.; Jiang, T.; Wang, J.; Chen, L.; Wei, B.; Li, Y.; Xu, G.; Wang, Z. Effects of different external fields on the microstructure and mechanical properties of novel Al-Cu-Li alloy during twin-roll casting. *Mat Sci Eng: A* **2019**, *757*, 14-22. DOI: https://doi.org/10.1016/j.msea.2019.04.079
24. Li, S.; Wei, B.; Yu, Ch.; Li, Y.; Xu, G.; Li, Y. Evolution of microstructure and properties during homogenization of the novel Al–Li alloy fabricated by electromagnetic oscillation twin-roll casting. *J Mater Research Tech* **2020**, *9*, 3304-3317. DOI: https://doi.org/10.1016/j.jmrt.2020.01.025

25. Grydin, O.; Stolbchenko, M.; Schaper, M.; Belejova, S.; Kralik, R.; Bajtosova, L.; Krivska, B.; Hajek, M.; Cieslar, M. New Twin-Roll Cast Al-Li Based Alloys for High-Strength Applications. *Metals* **2020**, *10*, 987. DOI: https://doi.org/10.3390/met10080987
26. Hajek, M.; Vesely, J.; Cieslar, M. Precision of electrical resistivity measurements. *Mat Sci Eng: A* **2007**, *462*, 339-342. DOI: https://doi.org/10.1016/j.msea.2006.01.175
27. Rodgers, B. I.; Prangnell, P. B. Quantification of the influence of increased pre-stretching on microstructure-strength relationships in the Al–Cu–Li alloy AA2195. *Acta Mater* **2016**, *108*, 55-67. DOI: https://doi.org/10.1016/j.actamat.2016.02.017
28. Slamova, M.; Karlik, M.; Rabaut, F.; Slama, P.; Veron, M. Differences in microstructure and texture of Al–Mg sheets produced by twin-roll continuous casting and by direct-chill casting. *Mater Charact* **2002**, *49*, 231-240. DOI: https://doi.org/10.1016/S1044-5803(03)00011-1
29. Bajtosova, L.; Grydin, O.; Stolbchenko, M.; Schaper, M.; Krivska, B.; Kralik, R.; Slapakova, M.; Cieslar, M. Phase identification in twin-roll cast Al-Li alloys. In proceedings of 31st International Conference on Metallurgy and Materials, METAL 2022**,** Brno, Czech Republic, 18-19. 05 2022.
30. Kim, J-H.; Yeun, J-H.; Chun, H-J.; Lee, R-J.; Too, J-T.; Yoon, J-H.; Lee, H-S. Effect of precipitates on mechanical properties of AA2195. *J Alloy Compd* **2016**, *669*, 187-198. DOI: https://doi.org/10.1016/j.jallcom.2016.01.229
31. Jin, Y.; Yu, H. Enhanced formability and hardness of AA2195-T6 during electromagnetic forming. *J Alloy Compd* **2022**, *890*, 161891. DOI: https://doi.org/10.1016/j.jallcom.2021.161891
32. Sahoo, S.; Ghosh, S. Microstructure evolution of eutectic Al–Cu strips by high-speed twin-roll strip casting process. *Appl Phys A – Mater* **2015**¸*121*, 45-50. DOI: https://doi.org/10.1007/s00339-015-9319-5
33. Zhang, Y.; Wang, J.; Chen, D.; Wang, B.; Zhang, C.; Wang, Z. Effects of cooling rates on microporosity in DC casting Al-Li alloy. *China Foundry* **2022**, *19*, 177-190. DOI: https://doi.org/10.1007/s41230-022-1183-2
34. Zhang, F.; Shen, J.; Yan, X.; Sun, J.; Sun, X.; Yang, Y. Homogenization heat treatment of 2099 Al–Li alloy. *Rare Metals* **2013**, *33*, 28-36. DOI: https://doi.org/10.1007/s12598-013-0099-9
35. Flemings, M. C. Solidification Processing. *Metall Trans* **1974**, *5*, 2121-2134. DOI: https://doi.org/10.1007/BF02643923
36. Ramirez-Vidaurri, L. E.; Castro-Roman, M.; Herrera-Trejo, M.; Fraga-Chavez, K. Secondary dendritic arm spacing and cooling rate relationship for an ASTM F75 alloy. *J Mater Res Tech* **2022**, *19*, 5049-5065. DOI: https://doi.org/10.1016/j.jmrt.2022.06.146